Porous Solids

DOI: 10.1002/anie.200503950

A Nanowire–Nanoparticle Cross-Linking Approach to Highly Porous Electrically Conducting Solids**

Nidhal N. Akl, Olga Trofymluk, Xiubin Qi, Jin Y. Kim, Frank E. Osterloh, and Alexandra Navrotsky**

As a result of their high surface-to-volume ratios, porous inorganic solids have found technological applications as

[*] N. N. Akl, X. Qi, J. Y. Kim, Prof. F. E. Osterloh
Department of Chemistry
University of California at Davis
One Shields Avenue, Davis, CA 95616 (USA)
Fax: (+1) 530-752-8995
E-mail: fosterloh@ucdavis.edu

O. Trofymluk, Prof. A. Navrotsky
Thermochemistry facility and NEAT ORU
University of California at Davis
One Shields Avenue, Davis, CA 95616 (USA)
Fax: (+1) 530-752-8995
E-mail: anavrotsky@ucdavis.edu

[**] This work was supported by a grant (CTS 04-27418) from the National Science Foundation. We thank Prof. Susan Kauzlarich for providing a furnace for the synthesis of starting materials.

Supporting information (full experimental details) for this article is available on the WWW under http://www.angewandte.org or from the author.

molecular sieves, ion exchangers, and catalysts.[1] Recent research in the area of porous solids has also led to materials that combine high surface areas with electrical conductivity.[2] These porous conductors are desirable components in batteries, sensors, fuel cells, capacitors,[3] and electrocatalysts.[4] Porous conductors are typically synthesized by chemical linkage of electrically conductive colloidal building blocks (e.g. V_2O_5)[5,6] and their precursors (e.g. resorcine),[7] or by applying conductive coatings (e.g. RuO_2)[4] to existing porous solids. Another approach is to introduce mobile ions into porous structures.[8,9] We describe herein a novel approach to metallic porous solids that is based on cross-linking $LiMo_3Se_3$ nanowires with Ag nanoparticles. $LiMo_3Se_3$ nanowires (for structure see bottom of Figure 1) can be obtained easily by exfoliation of the corresponding Chevrel phase.[10,11] Owing to their metallic properties[12,13] the nanowires have been investigated as components in electrically conducting composites,[14–17] as electrode materials for Li-battery applications,[18] and as analyte-detection devices in nanowire-film chemiresistors.[19] When an aqueous dispersion of $LiMo_3Se_3$ nanowires is added to an aqueous dispersion of citrate-coated silver nanoparticles (15 ± 5 nm), a gel forms within minutes (Figure 1). Further analysis (see below) shows that the gel is

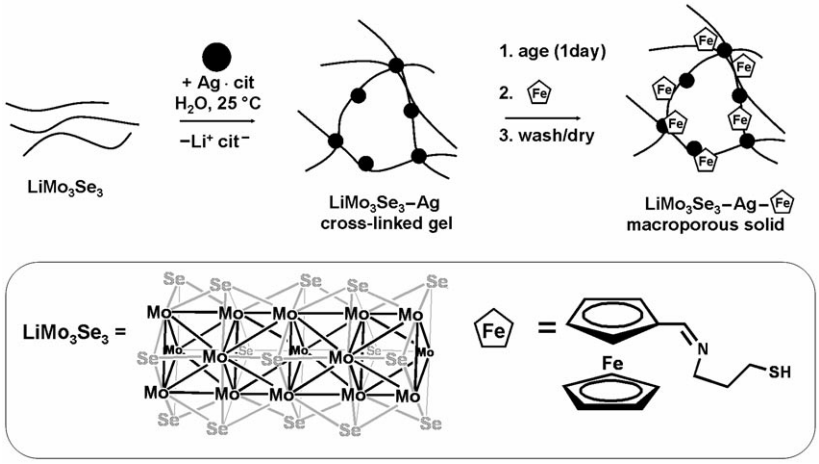

Figure 1. Synthesis and derivatization of the $LiMo_3Se_3$–Ag xerogel. cit = citrate; black circle = Ag nanoparticle. Li ions are omitted in the schematic structure of $LiMo_3Se_3$.

composed of silver nanoparticles that connect nanowire bundles through presumably covalent bonds between the silver and selenide ions. Similar covalent interactions occur in $LiMo_3Se_3$–Au and $LiMo_3Se_3$–CdSe composites.[17] These Ag–Se bonds form within seconds after mixing the reagents, as proven by the fact that centrifugation of a fresh reaction mixture leads to complete sedimentation of all inorganic materials whereas separate dispersions of silver nanoparticles and $LiMo_3Se_3$ nanowires are stable for weeks under similar conditions.

When left at 5 °C for 12 h, the gel shrinks to about 0.25 % of its original volume leaving behind a clear solution that is yellow owing to residual silver colloids (Figure 2 A). We postulate that the densification is driven by the tendency of the composite to maximize nanoparticle–nanowire interac-

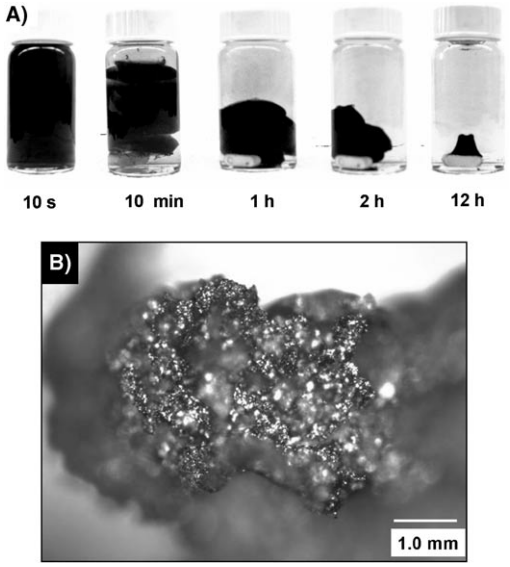

Figure 2. A) Evolution of the gel over time (note the stir bar at the bottom of the vial). B) Optical micrograph of the xerogel after drying in vacuum.

tions. The decrease of gel volume is accompanied by expulsion of pore fluid (syneresis) from the gel.[20] By decanting the clear mother liquor after 12 h and drying the deep-red solid in vacuo, one obtains a reflective solid with a volume of approximately 0.06 cm^3. The optical appearance of the xerogel (Figure 2 B) is indicative of metallic character.

Electron micrographs of a typical xerogel are shown in Figure 3 A–D. The images show that the solid contains a network of 2–6-μm large, irregularly shaped macropores. Furthermore, there are mesopores with sizes ranging from 15 to 130 nm (mean size 40 ± 21 nm, averaged over 45 mesopores) contained in the walls (Figure 3 D) of the xerogel. While these mesopores result from random packing of nanowires and nanoparticles, the macropores seem to form during expansion of the solvent (water) during vacuum drying. If the water is replaced by methanol prior to the drying step, the xerogels contain only mesopores with a mean size of 25 ± 10 nm (averaged over 35 mesopores). This observation demonstrates that water is essential for the formation of the macropores.

By altering the nanoparticle–nanowire stoichiometry in the synthesis, it is possible to tailor the size of the macropores of the xerogel. Figure 3 E shows pore-size distributions for gels assembled with the indicated stoichiometric ratios. The average pore size increases with increasing nanoparticle–nanowire ratio. This seems counterintuitive, as one might expect that increasing the number of cross-linkage points would produce a tighter-knit nanowire network. Instead, it seems that the pore sizes are determined by the kinetics of water evaporation. We hypothesize that the formation vapor bubbles is suppressed in the tightly knit and probably mechanically more robust mesh. Most of the water therefore evaporates from a small number of large water-vapor bubbles.

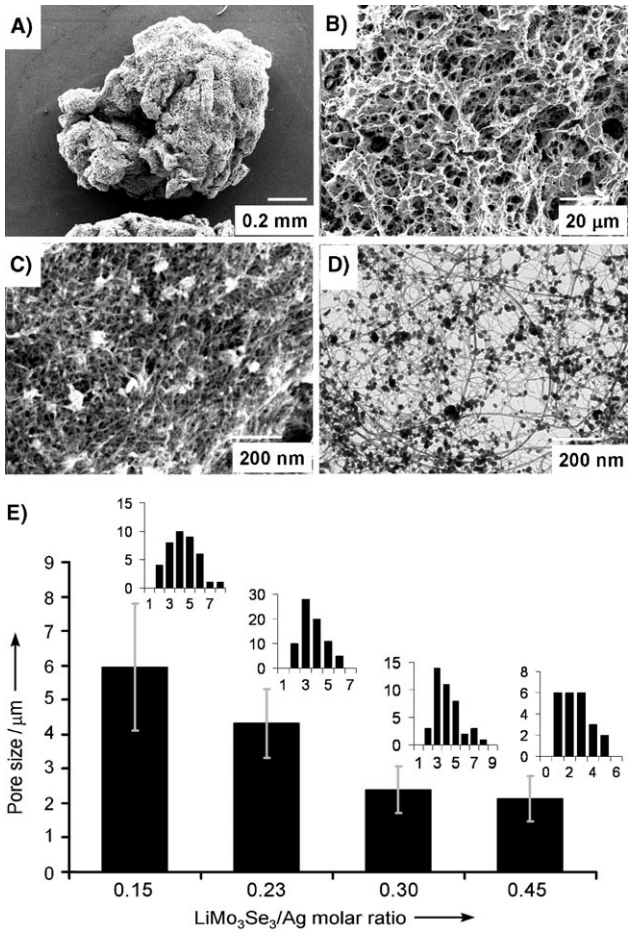

Figure 3. Variable magnification SEM (A–C) and TEM (D) images of the porous solid obtained with a $LiMo_3Se_3$/Ag ratio of 0.45. The thickness of the $LiMo_3Se_3$ nanowires (8.0 ± 1.7 nm) indicates the presence of bundles.[19] E) Effect of nanowire–nanoparticle stoichiometry on the mean mesopore sizes and the pore-size distributions (insets). Pore sizes were obtained from SEM images by measuring at least 80 pores in each sample. The error bars show standard deviations.

Smaller bubbles form (but in greater numbers) in the less tightly knit and mechanically less robust nanowire network, which eventually leads to a smaller mean pore size. This hypothesis is supported by the observation (from microscopy) that the number density of pores is smaller for xerogels with larger pores.

Nitrogen-adsorption porosimetry measurements were performed to complement the SEM/TEM analysis of the porous materials for pore sizes below 0.5 µm. For $LiMo_3Se_3$–Ag (0.23 mole ratio), the measurements reveal a rather wide pore-size distribution in the range 3–500 nm with an average pore size of 28 nm (see the Supporting Information). This value is in good agreement with the SEM data for the mesopores (40 ± 21 nm). The pore volume and the specific surface area (BET) were determined as $0.89\ cm^3\,g^{-1}$ and $760\ m^2\,g^{-1}$, respectively. These relatively large values indicate extensive porosity comparable with that in mesoporous silica.[21]

Resistance measurements reveal that the specific conductivity of the $LiMo_3Se_3$–Ag xerogel is $1.6\ S\,cm^{-1}$ (at 300 K). This value is significantly above that for conductive xerogels containing RuO_2 (10^{-3}–$10^{-7}\ S\,cm^{-1}$),[3,4] or MoO_3 ($10^{-5}\ S\,cm^{-1}$), and even exceeds the values for MoO_3–polypyrrol aerogel composites ($4 \times 10^{-3}\ S\,cm^{-1}$).[2] The low resistivity of the xerogel is attributable to the metallic character of its components and the connectivity of its framework.

A useful feature of the $LiMo_3Se_3$–Ag xerogels is their propensity for chemical derivatization with redox-active groups that become electrochemically accessible through the nanowire–nanoparticle network. Treatment of the gel with 3-{[(*E*)-ferrocenylmethylidene]amino}-1-propanethiol in methanol (as shown in Figure 2A) leads to a solid that contains approximately 1 mol% thiol (calculated on the basis of the Fe content observed with energy-dispersive spectroscopy). Control experiments show that the ferrocene thiol derivative also binds to pure $LiMo_3Se_3$ nanowires. We therefore conclude that thiol groups in the xerogel are bonded to both the silver and the nanowire portions.

Cyclic voltammograms (CVs) of $LiMo_3Se_3$–Ag and $LiMo_3Se_3$–Ag–Fc′ are shown in Figure 4 (Fc′ = thiol-functionalized ferrocene). The CV of $LiMo_3Se_3$–Ag reveals a broad

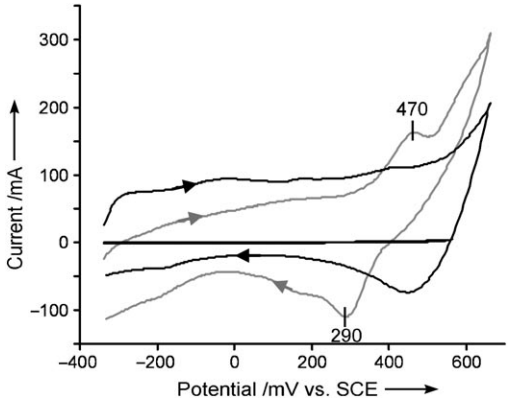

Figure 4. Cyclic voltammograms of porous monoliths (ca. 0.1 mg) in acetonitrile. $LiMo_3Se_3$–Ag (gray curve), $LiMo_3Se_3$–Ag–Fc′ (black curve). At around +0.50 V (vs. SCE) the nanowires of both composites are irreversibly oxidized.

feature that is consistent with capacitive charging under the applied potential. At potentials greater than +500 mV (vs. SCE), the nanowires in the xerogel are oxidized. The limited stability of $LiMo_3Se_3$ towards oxidation is a drawback of this material.

The CV of the thiol-functionalized solid is similar to that of the nonfunctionalized xerogel, except for the presence of additional redox features at +0.47 and +0.29 V, which correspond to the reversible oxidation process involving the ferrocene thiol derivative. The observed redox potential of +0.38 V (vs. SCE) is lower than that of the free thiol in CH_2Cl_2 (+0.49 V), which may be attributable to the different solvents (the potential for ferrocene moves from +0.46 V in CH_2Cl_2 to +0.40 V in the more polar MeCN).[22] The separation of the peaks by 0.18 V is likely caused by the finite mobility of the electrolyte NBu_4PF_6 in the porous network which limits the reversibility of the redox process. At

higher scan rates (ca. 100 mV s^{-1}) this effect leads to the complete disappearance of the thiol redox peaks. The CV shows that the electroactive groups inside the pores of the xerogel are electrically accessible through the metallic network.

In conclusion, we have shown that electrically conducting porous materials with adjustable pore sizes can be synthesized by using a new and very simple nanowire–nanoparticle cross-linking approach. The combination of high surface area, good electrical conductivity, and the ease of chemical derivatization make the material interesting as a high-surface-area electrode material for use in batteries or in electrocatalytic applications. The use of $LiMo_3Se_3$–Ag as a precursor to aerogels is currently under investigation.

Experimental Section

$LiMo_3Se_3$–Ag: To prepare the gel, variable volumes (0.1–0.3 mL) of a $LiMo_3Se_3$ nanowire solution (1.88 mM) were added dropwise to silver nanoparticle (15 ± 5 nm) solution (5.0 mL, 0.25 mM) in a 20-mL vial with rapid stirring. The resulting mixture was capped and stored in a refrigerator at 5 °C. After 12 h, the reddish gel had shrunk to about 0.25 % of its original volume. The clear aqueous layer was decanted, and the gel was washed carefully by addition of water to remove excess electrolytes. Drying in vacuo produced the metallic xerogel in quantitative yield (based on $LiMo_3Se_3$).

Thiol-functionalized $LiMo_3Se_3$–Ag: The $LiMo_3Se_3$–Ag gel as synthesized above was washed with methanol to remove residual water, then immersed in a solution of 3-{[(*E*)-ferrocenylmethylidene]amino}-1-propanethiol (5 mL, 0.125 M) in methanol. After 12 h, the gel was removed from the solution and carefully washed with three 20-mL aliquots of methanol. After the gel was soaked in fresh methanol for 12 h, the supernatant was decanted, and the solid was dried in a vacuum to obtain the thiol-modified xerogel.

Received: November 8, 2005
Revised: March 9, 2006
Published online: April 26, 2006

Keywords: Chevrel phases · gels · mesoporous materials · nanostructures

[1] N. Husing, U. Schubert, *Angew. Chem.* **1998**, *110*, 22; *Angew. Chem. Int. Ed.* **1998**, *37*, 23.
[2] D. R. Rolison, B. Dunn, *J. Mater. Chem.* **2001**, *11*, 963.
[3] J. W. Long, K. E. Swider, C. I. Merzbacher, D. R. Rolison, *Langmuir* **1999**, *15*, 780.
[4] J. V. Ryan, A. D. Berry, M. L. Anderson, J. W. Long, R. M. Stroud, V. M. Cepak, V. M. Browning, D. R. Rolison, C. I. Merzbacher, *Nature* **2000**, *406*, 169.
[5] F. Carn, N. Steunou, J. Livage, A. Colin, R. Backov, *Chem. Mater.* **2005**, *17*, 644.
[6] W. Dong, J. S. Sakamoto, B. Dunn, *Sci. Technol. Adv. Mater.* **2003**, *4*, 3.
[7] J. W. Long, B. M. Dening, T. M. McEvoy, D. R. Rolison, *J. Non-Cryst. Solids* **2004**, *350*, 97.
[8] T. Kamiya, H. Hosono, *Semicond. Sci. Technol.* **2005**, *20*, S92.
[9] O. Trofymluk, Y. Toda, H. Hosono, A. Navrotsky, *Chem. Mater.* **2005**, *17*, 5574.
[10] M. Potel, R. Chevrel, M. Sergent, J. C. Armici, M. Decroux, O. Fischer, *J. Solid State Chem.* **1980**, *35*, 286.
[11] J. M. Tarascon, F. J. DiSalvo, C. H. Chen, P. J. Carroll, M. Walsh, L. Rupp, *J. Solid State Chem.* **1984**, *54*, 290.
[12] L. Venkataraman, C. M. Lieber, *Phys. Rev. Lett.* **1999**, *83*, 5334.
[13] J. H. Song, B. Messer, Y. Y. Wu, H. Kind, P. D. Yang, *J. Am. Chem. Soc.* **2001**, *123*, 9714.
[14] J. K. Vassiliou, R. P. Ziebarth, F. J. Disalvo, *Chem. Mater.* **1990**, *2*, 738.
[15] J. H. Golden, F. J. Disalvo, J. M. J. Frechet, *Chem. Mater.* **1995**, *7*, 232.
[16] J. H. Golden, F. J. Disalvo, J. M. J. Frechet, J. Silcox, M. Thomas, J. Elman, *Science* **1996**, *273*, 782.
[17] F. E. Osterloh, J. S. Martino, H. Hiramatsu, D. P. Hewitt, *Nano Lett.* **2003**, *3*, 125.
[18] J. M. Tarascon, *J. Electrochem. Soc.* **1985**, *132*, 2089.
[19] X. B. Qi, F. E. Osterloh, *J. Am. Chem. Soc.* **2005**, *127*, 7666.
[20] C. J. Brinker, G. W. Scherer, *Sol–Gel Science*, Academic Press, New York, **1990**.
[21] D. Y. Zhao, Q. S. Huo, J. L. Feng, B. F. Chmelka, G. D. Stucky, *J. Am. Chem. Soc.* **1998**, *120*, 6024.
[22] N. G. Connelly, W. E. Geiger, *Chem. Rev.* **1996**, *96*, 877.

